

Sparse and low-rank approximations of large symmetric matrices using biharmonic interpolation

Javier S. Turek^{*1} and Alexander Huth^{*2}

¹Parallel Computing Lab, Intel Labs, Hillsboro, OR,
javier.turek@intel.com

²Helen Wills Neuroscience Institute, University of California,
 Berkeley, CA, alex.huth@berkeley.edu

May 13, 2022

Abstract

Symmetric matrices are widely used in machine learning problems such as kernel machines and manifold learning. Using large datasets often requires computing low-rank approximations of these symmetric matrices so that they fit in memory. In this paper, we present a novel method based on biharmonic interpolation for low-rank matrix approximation. The method exploits knowledge of the data manifold to learn an interpolation operator that approximates values using a subset of randomly selected landmark points. This operator is readily sparsified, reducing memory requirements by at least two orders of magnitude without significant loss in accuracy. We show that our method can approximate very large datasets using twenty times more landmarks than other methods. Further, numerical results suggest that our method is stable even when numerical difficulties arise for other methods.

1 Introduction

Symmetric matrices have many important roles in the machine learning field. These matrices are often used to describe pairwise relationships between samples in a dataset. In kernel-based methods, such as Support Vector Machines (SVM) or Kernel Ridge Regression (KRR), symmetric matrices represent the pairwise evaluation of data samples in kernel space. In other cases, like in Multidimensional

^{*}Equal contributors.

Scaling (MDS) or Isomap for manifold learning, these matrices represent geodesic distances in a manifold.

Given a dataset of n points, $\mathcal{O}(n^2)$ space is required to store a symmetric matrix in memory. Many algorithms require computations that execute in $\mathcal{O}(n^3)$ runtime. With growing datasets, these requirements quickly become intractable, limiting scalability and applicability. One solution is to compute a low-rank approximation of the symmetric matrix. While the best rank k approximation is given by the Singular Value Decomposition (SVD), its computation is impractical for large matrices. An alternative is the Nyström method, which computes a low-rank approximation by subsampling l columns from the dataset. For example, the work [1] exploits the Nyström method to obtain a low-rank approximation of a kernel matrix and speed up Kernel SVM. Similarly, Landmark MDS [2] uses sampling to approximate embeddings from multidimensional scaling.

The Nyström method has been broadly studied theoretically [3, 4] and empirically [5, 6, 7]. However, the Nyström method has some limitations in large-scale problems. For datasets with millions of data points, sampling even a small fraction could mean using $l = 10,000$ or more. The memory complexity of Nyström is $\mathcal{O}(nl)$, potentially reaching tens to hundreds of gigabytes. Furthermore, Nyström requires computing a pseudoinverse, which can lead to numerical instability. Recent work has addressed some of these disadvantages [8, 9], but scalability is still limited.

Both a strength and a weakness of the Nyström method is that it makes no assumptions about the structure of the data beyond low-rank. This makes Nyström useful for many applications, but limits its effectiveness when more is known about the structure of the symmetric matrix. Here we consider the case where the data reside in a smooth, low-rank manifold. How can a low-rank approximation take advantage of information about manifold structure? In this work we explore a novel method, biharmonic matrix approximation (BHA), that aims at exploiting these ideas. Similar to Nyström, our method samples a subset of points and computes a low-rank approximation of the symmetric matrix. Our method then uses a biharmonic interpolation operator to approximate each element in the symmetric matrix by interpolating from the sampled data. We further introduce a sparse version of the interpolation operator that drastically reduces space complexity for large data sets. Empirical evaluation shows that, for certain tasks, BHA has accuracy that is comparable to or better than Nyström and can offer substantial improvements in space, enabling better approximations for very large datasets.

2 Background

Given a dataset of n points, $\{\mathbf{x}_i\}_{i=1}^n$ with $\mathbf{x}_i \in \mathbb{R}^d$, we define the symmetric (but not necessarily positive semidefinite) matrix $\mathbf{K} \in \mathbb{R}^{n \times n}$ as follows

$$\mathbf{K}_{i,j} = f(\mathbf{x}_i, \mathbf{x}_j), \quad (1)$$

where $\mathbf{K}_{i,j}$ represents the element in row i and column j of the matrix \mathbf{K} , and $f(\cdot, \cdot)$ is a function calculated for a pair of data points. Further assume that $f(\cdot, \cdot)$ is symmetric for a pair of points, i.e., $f(\mathbf{x}_i, \mathbf{x}_j) = f(\mathbf{x}_j, \mathbf{x}_i)$. Some examples of $f(\cdot, \cdot)$ include the inner product of the pairs, radial basis function (RBF) and polynomial kernels used in kernel methods, or geodesic distance between points as in linear embedding methods.

2.1 Nyström approximation method

The Nyström method is a symmetric matrix approximation that has been successfully applied to machine learning problems on large datasets. The method requires one to sample a subset of l landmark points from the dataset and compute the submatrix $\mathbf{C} \in \mathbb{R}^{n \times l}$, which consists of the corresponding l columns of \mathbf{K} . The low-rank approximation is then obtained as

$$\tilde{\mathbf{K}}^{Nys} = \mathbf{C}\mathbf{W}^\dagger \mathbf{C}^\top, \quad (2)$$

where $\mathbf{W} \in \mathbb{R}^{l \times l}$ is the symmetric diagonal block corresponding to the columns and rows of \mathbf{K} for the landmarks, and \mathbf{W}^\dagger is its Moore-Penrose pseudoinverse.

The Nyström approximation requires $\mathcal{O}(nl + l^2)$ space for storing the matrices \mathbf{C} and \mathbf{W}^\dagger . The runtime is $\mathcal{O}(nlf)$ for the computation of \mathbf{C} , where f is the complexity of evaluating the kernel function $f(\cdot, \cdot)$, and $\mathcal{O}(l^3)$ for computing the pseudoinverse of \mathbf{W} . We note that the cost of computing $\mathbf{K}_{i,j}$ depends on the evaluation of $f(\cdot, \cdot)$ which is typically $\mathcal{O}(d)$, but could be higher for geodesic distances.

Nyström methods are most useful for Kernel Machines. There, the method is used to approximate the kernel with a low-rank decomposition. It has an additional benefit that computing the solution to a problem may reduce the computational complexity of the algorithms that solve it. For example, the Kernel Ridge Regression (KRR) solution is given by $\mathbf{w} = (\lambda \mathbf{I} + \mathbf{K})^{-1} \mathbf{y}$, where \mathbf{y}_i is the regression value for each data point \mathbf{x}_i . Using the Matrix Inversion Lemma, the inversion can be simplified to $\mathbf{w} = \left[\frac{1}{\lambda} \mathbf{I} - \frac{1}{\lambda} \mathbf{C} (\lambda \mathbf{I} + \mathbf{W}^\dagger \mathbf{C}^\top \mathbf{C})^{-1} \mathbf{W}^\dagger \mathbf{C}^\top \right] \mathbf{y}$, where there is only an inversion of a small l by l matrix. Therefore, the runtime complexity is reduced from $\mathcal{O}(n^3)$ with the original kernel \mathbf{K} to $\mathcal{O}(nl^2 + l^3)$ with the Nyström approximation of the kernel.

2.2 Biharmonic interpolation

Let g be a real- or vector-valued function defined on a smooth manifold \mathcal{M} embedded in \mathbb{R}^d . The manifold has an associated Laplace-Beltrami Operator (LBO), Δ , that depends on the Riemannian metric of the manifold [10] such that $\Delta g = \text{div}(\text{grad } g)$.

Now suppose that we are given $g(\mathbf{b}_i)$ for a set of l points, $\{\mathbf{b}_i\}_{i=1}^l$ with $\mathbf{b}_i \in \mathcal{M}$, and wish to interpolate $g(\mathbf{u}_i)$ at a different set of m points, $\{\mathbf{u}_i\}_{i=1}^m \in \mathcal{M}$. One solution is biharmonic interpolation, which finds a smooth function (i.e. one with continuous second derivative) that passes exactly through $g(\mathbf{b}_i)$ for all i .

Biharmonic interpolation is accomplished by finding a solution to the biharmonic equation $\Delta^2 g(\mathbf{u}) = 0$, subject to Dirichlet boundary conditions given by $g(\mathbf{b}_i)$.

In the discrete case the biharmonic operator, Δ^2 , is specified as the sparse matrix \mathbf{M} . We assume that the manifold consists exclusively of the data points \mathbf{b} and \mathbf{u} , and thus that \mathbf{M} is an $(l + m) \times (l + m) = n \times n$ matrix.

We can organize the discrete biharmonic operator \mathbf{M} so that the first l rows and columns correspond to \mathbf{b} , our known data points, and the last m rows and columns correspond to \mathbf{u} , the points at which we wish to interpolate g . Thus \mathbf{M} can be split up into four submatrices

$$\mathbf{M} = \begin{bmatrix} \mathbf{M}_{bb} & \mathbf{M}_{bu} \\ \mathbf{M}_{ub} & \mathbf{M}_{uu} \end{bmatrix}. \quad (3)$$

To find the interpolated values we solve for $\hat{g}(\mathbf{u})$ in the modified biharmonic equation

$$\mathbf{M}_{uu}\hat{g}(\mathbf{u}) = -\mathbf{M}_{ub}g(\mathbf{b}), \quad (4)$$

which is a fully specified, sparse linear system of equations.

3 Biharmonic matrix approximation

In the proposed method we use biharmonic interpolation to approximate a manifold-structured symmetric matrix \mathbf{K} . We exploit the fact that the manifold structure of \mathbf{K} is similar to that of the underlying dataset $\mathcal{X} = \{\mathbf{x}_i\}_{i=1}^n$. We assume that \mathcal{X} lives in a manifold \mathcal{M} whose biharmonic operator \mathbf{M} can either be computed directly or approximated.

The first step is to select \mathbf{b} , a set of l landmark points from the dataset \mathcal{X} , and create an interpolation operator \mathbf{P} that interpolates from \mathbf{b} to the entire manifold by solving Equation 4

$$\mathbf{P} = \begin{bmatrix} \mathbf{I}_l \\ -\mathbf{M}_{uu}^{-1}\mathbf{M}_{ub} \end{bmatrix} = \begin{bmatrix} \mathbf{I}_l \\ \mathbf{P}_u \end{bmatrix}, \quad (5)$$

where $\{\mathbf{u}_i\} = \mathcal{X} \setminus \{\mathbf{b}_i\}$ is the set of all non-landmark points, \mathbf{M}_{uu} is the submatrix of \mathbf{M} corresponding to \mathbf{u} , and \mathbf{M}_{ub} is the submatrix that crosses \mathbf{u} and \mathbf{b} . Note that \mathbf{P} depends only on \mathcal{X} , and not the function that produces \mathbf{K} from \mathcal{X} .

The second step is to compute $\mathbf{W} \in \mathbb{R}^{l \times l}$, the diagonal block of \mathbf{K} corresponding to the landmark points: $\mathbf{W}_{i,j} = f(\mathbf{b}_i, \mathbf{b}_j)$ for $1 \leq i, j \leq l$. The Biharmonic Matrix Approximation (BHA) is then obtained as

$$\tilde{\mathbf{K}}^{BHA} = \mathbf{P}\mathbf{W}\mathbf{P}^\top. \quad (6)$$

Algorithm 1 summarizes the computation of BHA. While BHA may appear structurally similar to Nyström, a critical difference is that BHA does not compute the pseudoinverse \mathbf{W}^\dagger . BHA can be thought of as performing two interpolation operations. First, the product $\mathbf{P}\mathbf{W}$ interpolates the function values

from the landmarks to all the points, approximating the $n \times l$ submatrix \mathbf{C} formed by the columns of \mathbf{K} corresponding to the landmarks. Right-multiplying by \mathbf{P}^\top then interpolates each row of $\mathbf{P}\mathbf{W}$ across the entire manifold, giving the full $n \times n$ approximation $\tilde{\mathbf{K}}^{BHA}$.

3.1 Obtaining the discrete biharmonic operator

In order to compute the interpolation operator \mathbf{P} one must first obtain the discrete biharmonic operator \mathbf{M} , which is given as [11]

$$\mathbf{M} = (\mathbf{V} - \mathbf{A})^\top \mathbf{D}^{-1} (\mathbf{V} - \mathbf{A}), \quad (7)$$

where \mathbf{D} is a diagonal matrix containing the ‘‘lumped mass’’ at each point in the manifold, \mathbf{A} is a weighted adjacency matrix, and \mathbf{V} is a diagonal matrix containing the sum of the adjacency weights for each datapoint $\mathbf{V}_{i,i} = \sum_j \mathbf{A}_{i,j}$ [10].

In some cases there are closed-form solutions for the lumped mass and weighted adjacency matrices. If \mathcal{X} takes the form of a triangular mesh embedded in 3-D space, the lumped mass $\mathbf{D}_{i,i}$ is one third of the total area of the triangles incident on point i , and the adjacency weight

$$\mathbf{A}_{i,j} = \frac{\cot(\alpha_{i,j}) + \cot(\beta_{i,j})}{2}, \quad (8)$$

where $\alpha_{i,j}$ and $\beta_{i,j}$ are the angles opposite the edge between points i and j [10, 12]. Similar solutions for \mathbf{D} and \mathbf{A} exist for point clouds [13] and quad meshes [14] in 3-D space. If \mathcal{X} is a graph, we set $\mathbf{D} = \mathbf{I}$, and set \mathbf{A} equal to the graph adjacency matrix, where $\mathbf{A}_{i,j} = 1$ if nodes i and j share an edge, and 0 otherwise.

When no closed-form solution is available, \mathbf{D} and \mathbf{A} must be estimated. Here we set $\mathbf{D} = \mathbf{I}$ and focus on estimating \mathbf{A} . First we transform the dataset \mathcal{X} into an undirected graph by connecting each point to its t nearest neighbors and then symmetrizing the connections, forming the set $\mathcal{N}(i)$ of neighbors to point i . We then use Stochastic Neighbor Embedding [15, 16] (SNE) to assign a weight to each connection. In SNE, one computes asymmetric conditional probabilities using a Gaussian kernel $p_{j|i} = e^{-\|\mathbf{x}_i - \mathbf{x}_j\|^2 / 2\sigma_i^2} / \sum_{k \in \mathcal{N}(i)} e^{-\|\mathbf{x}_i - \mathbf{x}_k\|^2 / 2\sigma_i^2}$. The bandwidth of the Gaussian kernel, σ_i , is chosen separately for each data point such that the perplexity of $p_{j|i}$ is equalized for all j [15]. The asymmetric SNE probabilities are then symmetrized to produce the weighted adjacency matrix,

$$\mathbf{A}_{i,j} = \frac{1}{2} (p_{j|i} + p_{i|j}). \quad (9)$$

SNE provides excellent performance relative to fixed-bandwidth Gaussian RBFs, and in practice requires far less hyperparameter tuning. We found that setting t large and perplexity to 20.0 produced good results across a range of datasets.

3.2 From dense to sparse

Analyzing the interpolation operator \mathbf{P} reveals some useful numerical properties. The coefficients in \mathbf{P} define weights that are used to interpolate values in \mathbf{W} in order to approximate elements $\mathbf{K}_{i,j}$. Intuitively, as the number of landmarks grows, the number of data points influenced by each landmark will shrink. In the limit of the number of landmarks approaching the total number of data points, $\mathbf{P} \rightarrow I$, and each data point is only influenced by a single landmark. Thus, even though biharmonic interpolation operators are not theoretically guaranteed to be sparse (i.e. they do not have compact support), empirically most entries in \mathbf{P} tend to be near zero. We demonstrate this behavior empirically in the supplemental materials to this paper.

Therefore, instead of computing the interpolation operator \mathbf{P} given in Equation (5), we propose to compute a sparse interpolation operator. We note that Equation (5) describes the solution to a system of linear equations to obtain \mathbf{P} . Therefore, we replace the matrix inversion in Problem (5) by a sparse coding problem of the form

$$\tilde{\mathbf{P}}_u = \arg \min_{\mathbf{P}_u} \|\mathbf{M}_{uu}\mathbf{P}_u + \mathbf{M}_{ub}\|_F^2 \quad \text{s.t.} \quad \|\mathbf{P}_u^{(i)}\|_0 \leq p \quad \forall i, \quad (10)$$

where the $\|\mathbf{x}\|_0$ is defined as the ℓ_0 -quasinorm that measures the number of non-zeros in a vector \mathbf{x} , \mathbf{P}_u is the submatrix of \mathbf{P} corresponding to the non-landmark points $\{u_i\}$, $\mathbf{P}_u^{(i)}$ is the i^{th} column of \mathbf{P}_u , and p is a scalar value. The sparse interpolation operator \mathbf{P}_{sparse} is then obtained by plugging the solution $\tilde{\mathbf{P}}_u$ into Equation (5). Problem (10) constrains the solution to be a sparse matrix $\tilde{\mathbf{P}}_u$ with at most p non-zeros per column.

Sparse coding is a combinatorial problem, so its solution is typically approximated using greedy methods or convex relaxations such as OMP [17] or LASSO [18]. However, in cases such as this where most entries in \mathbf{P} are already very close to zero, we can use the much cheaper Thresholding method [19] to approximate Problem (10). Noting that the matrix \mathbf{M}_{uu} is square and invertible, this method chooses the p biggest elements in magnitude from the dense solution for each column of \mathbf{P} . Each column of \mathbf{P}_{sparse} is solved separately, requiring $\mathcal{O}(n)$ memory to store one dense column of \mathbf{P} at a time, and $\mathcal{O}(n)$ runtime complexity to find the biggest p elements. Typically, we are interested in p_{row} , the average number of non-zeros per row. The relation between p and a p_{row} parameter is given as $p = (n-l)p_{row}/l$.

How big must p_{row} be in order for \mathbf{P}_{sparse} to be a good approximation of \mathbf{P} ? If a large p_{row} is required, then there are no memory or runtime benefits of using \mathbf{P}_{sparse} . However, since most elements in \mathbf{P} are close to zero, it seems likely that p_{row} does not need to be very large. Although we provide no theoretical proof, our empirical evaluation in Section 4 suggests that p_{row} can be considered a small constant number, usually, $p_{row} \leq 50$ for any acceptable number of landmarks for large datasets.

Algorithm 1 Biharmonic Matrix Approximation (BHA)

Input: Data points $\{\mathbf{x}_i\}_{i=1}^n$, with $\mathbf{x}_i \in \mathbb{R}^d$, number of landmarks l , the function $f(\cdot, \cdot)$ that defines \mathbf{K} .

Output: Interpolation operator $\mathbf{P} \in \mathbb{R}^{n \times l}$ (or \mathbf{P}_{sparse}), submatrix $\mathbf{W} \in \mathbb{R}^{l \times l}$ of the symmetric matrix \mathbf{K} .

- 1: **Preprocessing:**
 - 2: **if** Manifold is triangular mesh **then**
 - 3: Compute weighted adjacency matrix \mathbf{A} using Equation (8).
 - 4: Compute lumped mass matrix \mathbf{D} .
 - 5: **else**
 - 6: Find t Nearest Neighbors of each sample, $\mathcal{N}(\mathbf{x}_i)$.
 - 7: Compute symmetric adjacency matrix where (i, j) adjacent if $\mathbf{x}_i \in \mathcal{N}(\mathbf{x}_j)$ or $\mathbf{x}_j \in \mathcal{N}(\mathbf{x}_i)$.
 - 8: Compute SNE-weighted adjacency matrix using Equation (9).
 - 9: Set lumped mass matrix $\mathbf{D} = I$.
 - 10: **end if**
 - 11: Compute the biharmonic operator \mathbf{M} using Equation (7).
 - 12: **Low-Rank Approximation:**
 - 13: Draw the set of landmark points with an uniform distribution.
 - 14: Solve Problem (5) to compute \mathbf{P} (or Problem (10) for \mathbf{P}_{sparse}).
 - 15: Compute \mathbf{W} , the submatrix of \mathbf{K} for the landmarks.
-

3.3 Runtime and space complexity

To analyze the runtime and space complexity of BHA we divide the method into two steps: a preprocessing step that computes the biharmonic operator \mathbf{M} , and a step that computes the interpolation operator \mathbf{P} and the diagonal block matrix \mathbf{W} for the landmarks.

In the preprocessing step, we compute the lumped mass matrix \mathbf{D} , the adjacency matrix \mathbf{A} and the sum of adjacency weights \mathbf{V} in order to obtain the biharmonic operator \mathbf{M} . Matrices \mathbf{D} and \mathbf{V} are diagonal and can be computed with one pass over the adjacency matrix \mathbf{A} , which is also sparse. When the manifold \mathcal{M} is known from a mesh with at most t neighbors for each point, the adjacency matrix is given and there is no need for more computation or space than is required by these matrices, yielding a total runtime complexity $\mathcal{O}(nt^2)$ and space $\mathcal{O}(nt^2)$ to compute and store \mathbf{M} . Practically, t has a small value of a few up to tens of neighbors per data point, such that still $t^2 \ll n$. When the manifold is not given, one must first estimate the biharmonic operator. Using the t Nearest Neighbors of each data point one can create a graph containing $\mathcal{O}(nt)$ edges (or non-zeros) in \mathbf{A} in $\mathcal{O}(dnt \log(t))$ time [20], including the weighted adjacency matrix. Thus the preprocessing step has a total runtime complexity of $\mathcal{O}(nt^2)$ and needs $\mathcal{O}(nt^2)$ space (this is an upper bound on the number of non-zeros; in practice, we found behavior closer to $\mathcal{O}(nt)$). In particular, we note that the preprocessing step is independent of the landmarks. Therefore,

it can be computed once and its outcome, the biharmonic operator \mathbf{M} , can be reused for different landmarks at no additional cost.

In the low-rank approximation step we draw a set of landmark points and then compute the interpolation operator \mathbf{P} and the matrix \mathbf{W} . Computing \mathbf{P} requires solving the system of linear equations described in (4). There are l right hand side vectors and the system has $n - l$ equations. As \mathbf{M} is a sparse matrix with $\mathcal{O}(n)$ non-zeros (assuming $t \ll n$), Equation (4) can be solved with sparse linear solvers in $\mathcal{O}(T_P nl)$, where T_P is the number of iterations needed to converge to a specific accuracy. Alternatively, we can compute the sparse Cholesky decomposition of \mathbf{M}_{uu} and then solve for the l right hand side vectors, having a runtime complexity $\mathcal{O}(n^{1.5} + nl)$. In the dense case, computing \mathbf{P} requires $\mathcal{O}(nl)$ space. In the sparse case, using p_{row} non-zeros per row with $p_{row} < l$ and practically constant, the space is reduced to $\mathcal{O}(np_{row})$ non-zeros. Computing sparse columns adds no cost. Eventually computing the submatrix \mathbf{W} of \mathbf{K} requires $\mathcal{O}(l^2 f)$ and $\mathcal{O}(l^2)$ space. It is worth noting that, despite a higher runtime complexity of $\mathcal{O}(\max\{dnt \log(t), nt^2\} + T_P nl + l^2 f)$ compared to Nyström, the method has a lower space complexity of $\mathcal{O}(\max\{np_{row} + l^2, nt^2\})$. This allows BHA to obtain low-rank approximations for larger datasets.

4 Experimental results

We empirically evaluate several variations of BHA and compare to Nyström in terms of both accuracy and runtime. In the first experiment we compare BHA and Nyström approximations of manifold geodesic distance matrices, both when the biharmonic operator \mathbf{M} is known to BHA and when \mathbf{M} needs to be estimated. In the second experiment we study the relationship between sparseness and approximation error, comparing BHA with dense \mathbf{P} to BHA with sparse \mathbf{P} and varying degrees of sparsity. In the third experiment we compare BHA and Nyström on a very large dataset where Nyström is impractical due to memory constraints. In the fourth experiment (see supplemental materials) we show that BHA beats Nyström in terms of runtime for an ensemble of kernel regression tasks.

For experiments we use five datasets. *Swiss Roll* is a synthetic dataset consisting of $n = 5,000$ 2-D data points embedded in 3-D. Stanford *Bunny* is a 3-D mesh with $n = 14,290$ points. *Brain 150K* is a 3-D mesh with $n = 151,191$ points, and *Brain 7K* is a downsampled version with $n = 7,502$ points. *roadNet-CA* is a graph of California road intersections [21] with $n = 1,957,027$ points.

All experiments were run on a system with two Intel Xeon E5-2699v3 processors (36 cores in total) with 128 GB of physical memory and running Linux. The code was implemented in Python with optimized and parallelized NumPy and SciPy modules. In particular, the Biharmonic Approximation method was implemented with k-Nearest Neighbors from Scikit-Learn, and sparse Cholesky decomposition from Scikit-Sparse. Geodesic distances were computed using the approximate geodesics in heat method [12] as implemented in pycortex [22].

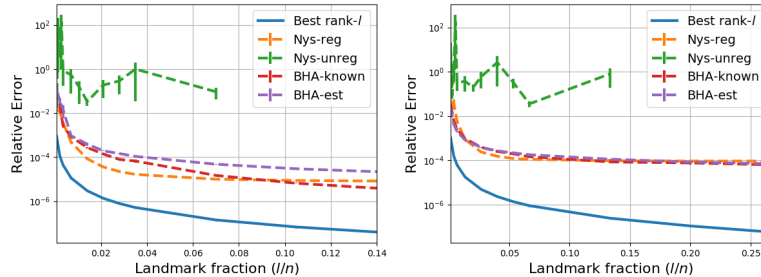


Figure 1: Accuracy comparison for BHA and Nyström on *Bunny* (left) and *Brain 7K* (right) datasets. BHA with known manifold outperforms Nyström for $l/n > 0.09$ for *Bunny* and > 0.11 for *Brain 7K*. Both BHA-known and Nys-reg outperform BHA-est for most of the l/n values. Nys-unreg is orders of magnitude worse for all tests.

4.1 Approximation with known manifold

One task for which BHA seems well suited is approximating a mostly-smooth kernel function, such as geodesic distance, applied to a 3-D manifold. In this task the data points $\{\mathbf{x}_i\} \in \mathcal{M} \subset \mathbb{R}^3$ and $\mathbf{K}_{i,j} = \|\mathbf{x}_i - \mathbf{x}_j\|_{\mathcal{M}}$, the geodesic distance between \mathbf{x}_i and \mathbf{x}_j across the manifold \mathcal{M} . Applying BHA to this task allows us to ask two questions. First, how does the accuracy of BHA on this task compare to Nyström? Second, how much accuracy is lost when we estimate the biharmonic operator \mathbf{M} using a t -Nearest Neighbor graph rather than computing \mathbf{M} exactly using Eq. (8)?

To answer these questions we examine the *Bunny* and *Brain 7k* datasets using three methods: BHA with known \mathbf{M} (BHA-known), BHA with estimated \mathbf{M} (BHA-est), and Nyström. For BHA-est we use $t = 20$ neighbors and compute a weighted adjacency matrix using SNE with perplexity 20.0. Both BHA methods use dense \mathbf{P} . For each method and dataset we measure the squared relative approximation error $\varepsilon(\tilde{\mathbf{K}}) = \|\tilde{\mathbf{K}} - \mathbf{K}\|_F^2 / \|\mathbf{K}\|_F^2$ using $l = 10 \dots 2000$, and average over 10 repetitions of this procedure, each time drawing different landmarks. We also computed the best rank- l approximation of \mathbf{K} using SVD, giving a lower bound on the approximation error. Occasional poor conditioning of the pseudoinverse \mathbf{W}^\dagger caused Nyström approximations to diverge (Nys-unreg). Therefore we recomputed Nyström excluding small singular values ($< 10^{-4} \sigma_{max}$) from the pseudoinverse to deal with these instabilities (Nys-reg). Note that this adds a hyperparameter to Nyström and bounds its accuracy.

The results of this experiment are shown in Figure 1. First, we found that the accuracy of BHA is very similar to regularized Nyström for most numbers of landmarks. With very large numbers of landmarks, BHA-known slightly outperforms the other methods. However, BHA-known has no hyperparameters

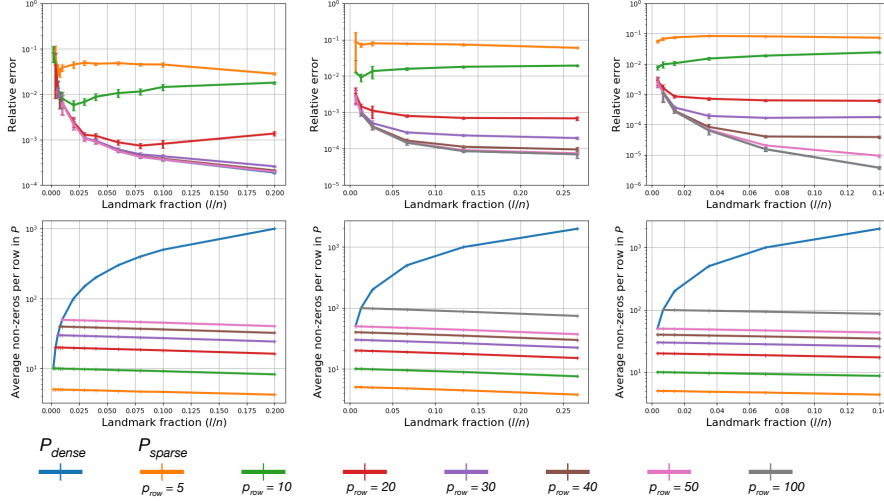


Figure 2: Accuracy comparison for BHA with dense and sparse interpolation operators. The sparse operator is computed for values of $p_{row} = 10 \dots 100$. The top row shows the error as a function of the fraction of landmarks l/n . The bottom row shows the average number of non-zeros per row for the same fraction of landmarks. The results are for *Swiss Roll* (left), *Brain 7K* (center), *Bunny* (right). For $p_{row} = 50$, sparse BHA gives very accurate approximations in all datasets.

that require tuning, unlike Nyström (which fails here unless regularized) and BHA-est. Unregularized Nyström (Nys-unreg) performs much worse than the other methods.

Second, we found only a modest difference between BHA-known and BHA-est. For the *Bunny* dataset, BHA-known is better overall, while for the *Brain 7k* dataset there is no consistent difference. This suggests that there is little penalty for estimating \mathbf{M} .

Finally, overall we saw that both BHA methods had between two and three orders of magnitude higher error than the best rank- l approximation across a broad range of l . Still, error for BHA fell to about 1 part in 100,000 with the highest l tested, demonstrating that BHA is relatively successful on these examples. One issue hampering accuracy is that BHA only outputs smooth functions, whereas geodesic distance functions form sharp cusps at distance zero and, for closed meshes, at the antipode of each point.

4.2 Sparsity of the interpolation operator \mathbf{P}

In Section 3.2 we described how to obtain \mathbf{P}_{sparse} , a sparse approximation of the interpolation operator \mathbf{P} . Here, we evaluate the performance of the sparse

operator and its savings in space. We compute low-rank approximations using sparse BHA with varying values of p_{row} between 5 and 100 non-zeros per row, and also using dense BHA. The operator \mathbf{P}_{sparse} is obtained by thresholding each column as described in Section 3.2. Performance is again measured using squared relative approximation error. For datasets with a defined mesh (*Bunny* and *Brain 7K*), \mathbf{K} is computed with geodesic distances. Otherwise (*Swiss Roll*), \mathbf{K} is defined with pairwise Euclidean distances and use $t = 10$ neighbors for the NN graph in BHA.

We compare performance as a function of the percentage of the chosen landmarks points in Figure 2 (top row) for selected datasets. The plots show that accuracy for \mathbf{P}_{sparse} is very similar to the dense version with values $p_{row} > 40$ in all datasets. It is worth mentioning that in large datasets the fraction of landmarks used to approximate \mathbf{K} will be lower due to growing memory requirements. When the landmark fraction is 7% or less, $p_{row} = 50$ approximates the dense interpolation operator with high accuracy. But as the landmark fraction increases, the p_{row} necessary to approximate the dense operator does not seem to grow quickly. In Figure 2 (bottom row) we show the average number of non-zeros per row in \mathbf{P} . Using \mathbf{P}_{sparse} can reduce memory requirements by two orders of magnitude over dense BHA while achieving nearly identical approximation error.

4.3 Very large dataset

The greatest benefit of BHA over Nyström is that \mathbf{P} can be sparse, making it possible to approximate much larger datasets in the same amount of memory. Here we used both methods to approximate the matrix of shortest paths through the graph given by *roadNet-CA*. Path length is computed as the number of edges between each pair of intersections using Dijkstra’s algorithm. For BHA we took \mathbf{A} to be the connectivity matrix, where $\mathbf{A}_{i,j} = 1$ if points i and j share an edge.

Because the full \mathbf{K} matrix is too large to compute in its entirety, we approximate the accuracy of each method by testing only 1,000 randomly selected rows of \mathbf{K} . The large size of the dataset also limits the number of landmarks that can be used for each method. For Nyström we are able to use up to 5,000 landmarks before hitting memory limits, while for sparse BHA with p_{row} we are able to use 100,000 or more. Results are shown in Figure 3. The accuracy of BHA surpasses Nyström, even when BHA uses less memory. BHA is also able to use many more landmarks in the same memory, thanks to the sparsity of \mathbf{P} .

5 Conclusions

The BHA method developed here offers a sparse alternative to approximation methods like Nyström. Sparsity allows BHA to be efficient in both memory and evaluation time. The accuracy of BHA is comparable to Nyström, but more stable, for manifold-based problems such as approximating geodesic distances across 3-D meshes. To improve BHA and make it competitive for other cases, a promising direction is better handling localized non-smooth regions that appear

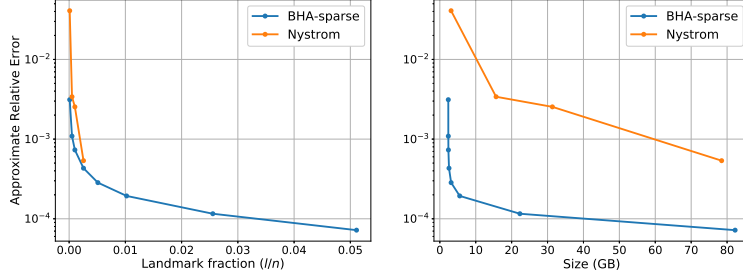


Figure 3: Accuracy comparison for BHA and Nyström on the 1,957,027 point *roadNet-CA* dataset. Error is approximated using 1000 randomly selected rows from the $1,957,027 \times 1,957,027$ distance matrix \mathbf{K} . Nyström is run with up to 5,000 landmarks. Sparse BHA (with $p_{row} = 100$) is able to be run with 100,000 landmarks. Plots show accuracy as a function of fraction of landmarks (left), and as a function of total size of the matrices in gigabytes (right).

for example, near zero in geodesic distance functions. Additionally, improvements to the construction of the Nearest Neighbor graph and weighted adjacency matrix, could benefit both runtime and approximation accuracy. Ultimately, more research is needed to provide theoretical guarantees on the performance and stability of the BHA. Nevertheless, the results in this work show that BHA is beneficial and immediately applicable to approximating symmetric matrices on large datasets.

Appendix

A Properties of the interpolation operator \mathbf{P}

Let us recall from Section 2 the definition of the interpolation operator \mathbf{P}_b for a set of landmarks $\{\mathbf{b}_i\}$:

$$\mathbf{P} = \begin{bmatrix} \mathbf{I}_l \\ \mathbf{P}_{b \rightarrow u} \end{bmatrix}, \quad (11)$$

where $\mathbf{P}_{b \rightarrow u}$ is computed solving the linear system of equations

$$\mathbf{M}_{uu} \mathbf{P}_{b \rightarrow u} = -\mathbf{M}_{ub}. \quad (12)$$

One interesting property of \mathbf{P} is that each row sums to exactly 1. This follows from the fact that every row and column of \mathbf{M} sums to exactly zero, and thus for the k -th row of \mathbf{M}_{uu} and \mathbf{M}_{ub}

$$\mathbf{M}_{uu}^{(k)} \mathbf{1}_m = -\mathbf{M}_{ub}^{(k)} \mathbf{1}_l$$



Figure 4: Images of the 3D datasets. From left to right: *Swiss Roll*, *Stanford Bunny*, and *Brain 150K*.

where $\mathbf{1}_q$ is a column vector of ones of length q . From (12) we have

$$\mathbf{M}_{uu}^{(k)} \mathbf{P}_{b \rightarrow u} = -\mathbf{M}_{ub}^{(k)}$$

Multiplying each side by $\mathbf{1}_l$ yields

$$\begin{aligned} \mathbf{M}_{uu}^{(k)} \mathbf{P}_{b \rightarrow u} \mathbf{1}_l &= -\mathbf{M}_{ub}^{(k)} \mathbf{1}_l \\ \Rightarrow \mathbf{M}_{uu}^{(k)} \mathbf{P}_{b \rightarrow u} \mathbf{1}_l &= \mathbf{M}_{uu}^{(k)} \mathbf{1}_m \\ \Rightarrow \mathbf{P}_{b \rightarrow u} \mathbf{1}_l &= \mathbf{1}_m \end{aligned}$$

Because values in \mathbf{P}_b can be either positive or negative, this means that the interpolated value at each \mathbf{u}_i is an affine combination of the values $f(\mathbf{b})$.

B Datasets

In Figure 4 we present images of the datasets that are embedded in three dimensions that were used for the experimental results in Section 4.

C Visual analysis of the values of \mathbf{P}

In Section 3.2, we discussed why many of the values in the interpolation operator \mathbf{P} tend to zero. We describe here additional experiments that demonstrate this behavior graphically. Let us consider first, the following example. We draw $n = 5,000$ data points from a rectangle in \mathbb{R}^2 and embed them in the swiss roll manifold in \mathbb{R}^3 . We define $f(\mathbf{x}_i, \mathbf{x}_j) = \|\mathbf{x}_i - \mathbf{x}_j\|_2$, the Euclidean distance between the points in \mathbb{R}^3 . Then, we compute the interpolation operator \mathbf{P} and the distances \mathbf{W} between $l = 100$ landmark points drawn uniformly. Figure 5 depicts the histogram of the values in \mathbf{P} . The bin including the range $[-0.00495, 0.00495]$ contains approximately 82.75% of the 500,000 available elements¹. This suggests that most of the values in the operator \mathbf{P} are very small or zero.

¹The identity block in \mathbf{P} corresponding to the landmarks has only 9,900 zeros and 100 ones, which is small relative to the operator size.

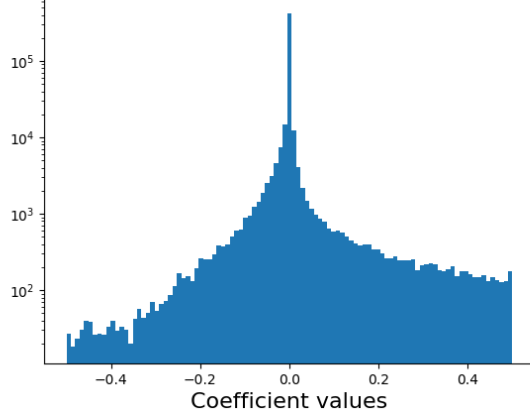


Figure 5: Histogram representing the distribution of values in the interpolation operator \mathbf{P} obtained from the dataset *Swiss Roll* with $l = 100$ landmarks. The number of near-zero values is an order of magnitude bigger than the non-zero values.

Next, we explore visually the influence of the number of landmarks l on the values of a column of \mathbf{P} . For this purpose, we use the *Stanford Bunny* dataset and we use BHA to approximate geodesic distances. First, we compute the interpolation matrix \mathbf{P} for $l = 30$ landmarks. We select a column from \mathbf{P} and plot the values in the 3D bunny (see Figure 6 top). The visible landmark points appear as black dots. Red areas represent higher positive values, whereas blue areas the negative ones. Zero or near-zero values are represented with white. Then we draw additional landmarks and recompute \mathbf{P} . Figure 6 in the middle shows the same column of \mathbf{P} projected on the bunny mesh when $l = 70$ landmarks are selected for BHA, and the bottom figure when $l = 300$ landmarks are drawn.

One can see that as the number of landmarks grows, the influence of the selected landmark on the nearby points reduces as illustrated by the shrinking red and blue areas. As a direct consequence of this shrinking, there are wider white areas of almost zero values for the particular column of \mathbf{P} , suggesting that its influence is almost null for many data points and it effectively can be sparsified.

D Thresholding algorithm

In Section 3.2, we show how we achieve a sparse interpolation operator \mathbf{P}_{sparse} by solving a sparse coding problem. For the sake of completeness, we describe in here the Thresholding algorithm that is used for this purpose. The thresholding algorithm is used to compute one column of \mathbf{P} at a time, thus we explain how to compute it for one column. Given a vector \mathbf{b} and a matrix \mathbf{A} as input, the

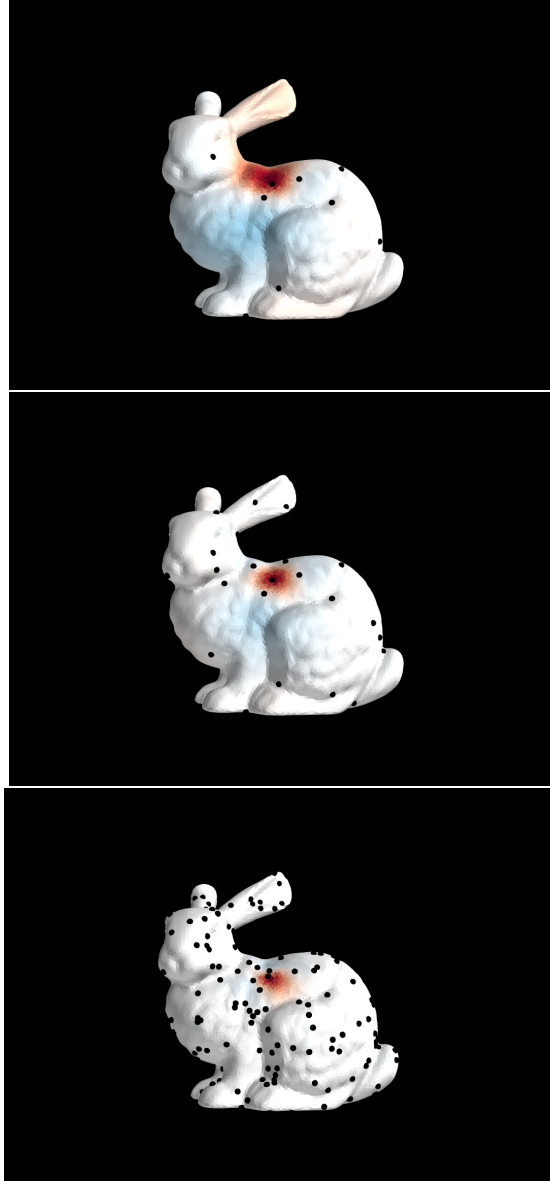


Figure 6: The values of a selected column of the interpolation operator \mathbf{P} projected back to the *Bunny* mesh when the \mathbf{P} is computed with $l = 30$ (top), $l = 70$ (middle), and $l = 300$ landmarks (bottom). Black dots show landmarks. Red areas represent positive values, blue are negative values, and white for near-zero values. As the number of landmarks increases, most of the values for this column of \mathbf{P} go to zero.

sparse coding problem looks for sparse solution to the problem

$$\min_x \frac{1}{2} \|\mathbf{A}\mathbf{x} - \mathbf{b}\|_2^2 \quad \text{s.t.} \quad \|\mathbf{x}\|_0 \leq p. \quad (13)$$

In the case of BHA, \mathbf{A} is a square invertible matrix and Problem (13) can be solved with the Thresholding method by first computing $\mathbf{z} = \mathbf{A}^{-1}\mathbf{b}$. Then, we find S the set of indexes of the biggest elements in magnitude in \mathbf{z} . We use the Selection procedure [23] to find them in $\mathcal{O}(n)$ and avoid sorting. Last, we compute the solution by setting the values of elements in \mathbf{x} for the indexes in S to those of \mathbf{z} , and the other elements to zero. Algorithm 2 summarizes these steps.

Algorithm 2 Thresholding Algorithm for BHA

Input: A vector $\mathbf{b} \in \mathbb{R}^m$, a square invertible matrix $\mathbf{A} \in \mathbb{R}^{m \times m}$, and a cardinality p .

Output: A vector $\mathbf{x} \in \mathbb{R}^n$ with at most p non-zeros, such that approximates a solution to (13).

- 1: Compute $\mathbf{z} = \mathbf{A}^{-1}\mathbf{b}$.
 - 2: Find the set S of the p indexes with biggest magnitude $|\mathbf{z}|$ using the Selection algorithm.
 - 3: Compute vector \mathbf{x} such that $\mathbf{x}_i = \mathbf{z}_i$ if $i \in S$, or $\mathbf{x}_i = 0$ otherwise.
-

E Row sparsification

In the main manuscript we described how to obtain a sparse interpolation operator \mathbf{P}_{sparse} by sparsifying the columns of $\mathbf{P}_{b \rightarrow u}$. Another option would be to sparsify $\mathbf{P}_{b \rightarrow u}$ by rows. This would require to replace the constraint in sparse coding problem to

$$\begin{aligned} \tilde{\mathbf{P}}_{b \rightarrow u} &= \arg \min_{\mathbf{P}_{b \rightarrow u}} \|\mathbf{M}_{uu}\mathbf{P}_{b \rightarrow u} + \mathbf{M}_{ub}\|_F^2 \\ \text{s.t.} \quad &\|\mathbf{P}_{(i)b \rightarrow u}\|_0 \leq p_{row} \quad \forall i, \end{aligned} \quad (14)$$

where the ℓ_0 -quasinorm is applied to the rows $\mathbf{P}_{(i)b \rightarrow u}$ of $\mathbf{P}_{b \rightarrow u}$. In this case, applying a thresholding algorithm by row requires to maintain a min-heap with the biggest p_{row} elements per row. While the memory consumption is the same $\mathcal{O}(n)$, the runtime becomes $\mathcal{O}(n \log(p_{row}))$. Assuming $p_{row} \ll n$ or even constant, sparsifying by columns or rows has almost the same complexity.

In Figure 7, we show the results of the experiment in Section 4.2 when \mathbf{P}_{sparse} is computed following Problem (14). The results show similar behavior as those in Section 4.2, with slightly better results for lower p_{row} values when \mathbf{P}_{sparse} column is sparsified by columns.

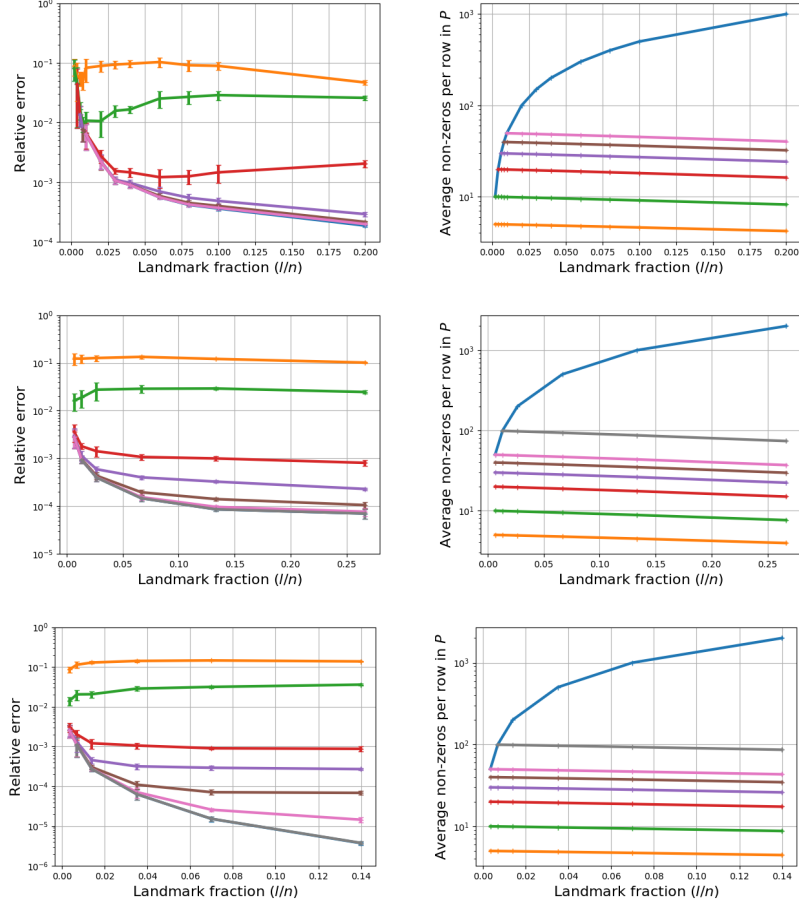


Figure 7: Relative approximation error comparison for BHA with dense and sparse interpolation operators. The sparse operator is computed thresholding the biggest $p_{row} = 10 \dots 100$ values in magnitude per row. The figures on the left depict the error as a function of the fraction of landmarks l/n . The figures on the right show the average number of non-zeros per row. The results are for *Swiss Roll* (top), *Brain 7K* (middle), *Bunny* (bottom). For $p_{row} = 50$, the sparse BHA exhibits very accurate approximations in all datasets.

F Runtime comparison

In deployed machine learning systems, is very common to use an ensemble of methods to boost inference accuracy. In this experiment we simulate training a regression system consisting of an ensemble of q kernel machines. We assume that the models are trained with the same data points and the difference between

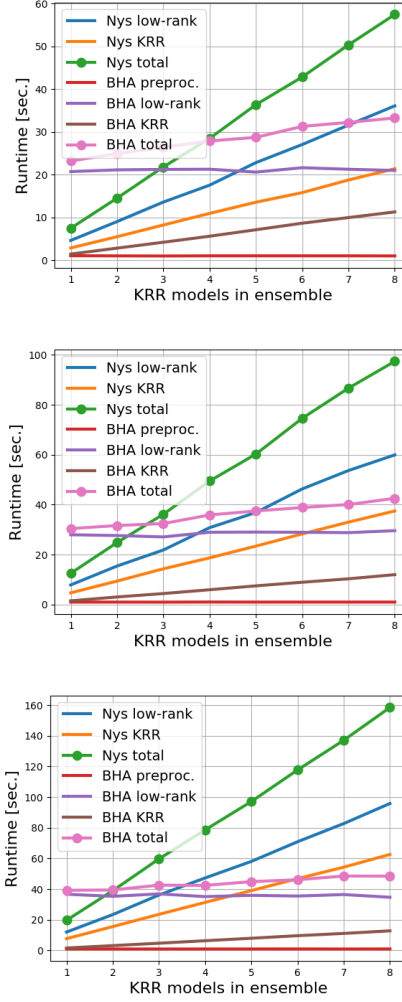


Figure 8: Runtime comparison between BHA and Nyström for training ensembles of KRR models with 1,000 (top), 1,500 (middle), and 2,000 (bottom) landmark points.

models is only the kernel functions. We measure the time required to compute the low-rank matrix approximation and the time to solve the KRR given in Section 2.1. We set values of $q = 1 \dots 8$ models and average the timings over 10 repetitions of the experiment. We compare the Nyström and Bi-harmonic matrix approximation on the *Brain 150K* dataset. The number of landmarks l for both methods is set to 1,000, 1,500, and 2,000. The Nyström method must

recompute the matrix approximation for every kernel machine. On the other hand, BHA needs only to recompute the matrix \mathbf{W} (assuming same landmarks across models), but requires an additional preprocessing step and must compute \mathbf{P}_{sparse} for the first kernel machine. Arbitrarily, we choose RBF kernels with different width parameter γ_q for the kernel machines. We compute the sparse version of BHA with approximately $p_{row} = 50$ non-zeros per row.

The runtime results are presented in Figure 8. When $l = 1,000$ landmarks are used (Figure 8 top), BHA is faster than Nyström after $q = 5$ kernel machines are used. In Figure 8 (middle), one can see that with $q = 3$ models in the ensemble, BHA has further lower total runtime than Nyström. As the number of landmarks increases in Figure 8 (bottom), the crossing point where BHA is faster than Nyström moves to lower values of q . Therefore, we expect BHA to be faster for very large datasets even for a single KRR. The reason that we see a cross-over point in Figure 8 is that Nyström must recompute the columns \mathbf{C} and the pseudoinverse \mathbf{W}^\dagger for each kernel, whereas BHA has a higher computational costs for the first KRR model and then is reduced to only recomputing \mathbf{W} for subsequent kernels. The difference between the methods is magnified as the dense matrix \mathbf{C} size grows. Furthermore, there is a memory benefit for BHA. For example, with $l = 1500$ landmarks BHA requires approximately 140 MB, whereas Nyström utilizes about 1.8 GB to store a *single* low-rank approximation.

In addition, we ran this experiment on the *MNIST* dataset [24] (data not shown). In this case, the preprocessing time for BHA was dominated by the computation of the Nearest Neighbors method with $t = 10$ (>400 sec.), while the remaining parts took only a few seconds. Consequently, the timings were always better for Nyström. The main reason for the lengthy preprocessing is the large number $d = 784$ of features as compared to other datasets that we tested. However, we note that this could be improved significantly by using approximate Nearest Neighbor methods, such as Locality Sensitive Hashing Forest [25]. Also, the current implementation could be further optimized. Improving the graph estimation for large dimension d is left for future work.

References

- [1] C. K. I. Williams and M. Seeger. Using the nyström method to speed up kernel machines. In T. K. Leen, T. G. Dietterich, and V. Tresp, editors, *Advances in Neural Information Processing Systems 13*, pages 682–688. MIT Press, 2001.
- [2] J. B. Tenenbaum. A global geometric framework for nonlinear dimensionality reduction. *Science*, 290(5500):2319–2323, Dec. 2000.
- [3] P. Drineas and M. W. Mahoney. On the nyström method for approximating a gram matrix for improved kernel-based learning. *J. Mach. Learn. Res.*, 6:2153–2175, Dec. 2005.

- [4] S. Kumar, M. Mohri, and A. Talwalkar. Sampling methods for the nyström method. *J. Mach. Learn. Res.*, 13:981–1006, Apr. 2012.
- [5] C. Cortes, M. Mohri, and A. Talwalkar. On the impact of kernel approximation on learning accuracy. In Y. W. Teh and M. Titterton, editors, *Proceedings of the 13th International Conference on Artificial Intelligence and Statistics (AISTATS 2010)*, volume 9, pages 113–120, 2010.
- [6] M. Li, J. T. Kwok, and B.-L. Lu. Making large-scale nyström approximation possible. In Johannes Fürnkranz and Thorsten Joachims, editors, *Proceedings of the 27th International Conference on Machine Learning (ICML-10)*, pages 631–638, Haifa, Israel, Jun. 2010. Omnipress.
- [7] A. Talwalkar, S. Kumar, M. Mohri, and H. Rowley. Large-scale svd and manifold learning. *Journal of Machine Learning Research*, 14:3129–3152, 2013.
- [8] S. Si, C.-J. Hsieh, and I. Dhillon. Memory efficient kernel approximation. In Eric P. Xing and Tony Jebara, editors, *Proceedings of The 31st International Conference on Machine Learning (ICML-14)*, pages 701–709, Jun. 2014.
- [9] M. Li, W. Bi, J. T. Kwok, and B. L. Lu. Large-scale nyström kernel matrix approximation using randomized svd. *IEEE Transactions on Neural Networks and Learning Systems*, 26(1):152–164, Jan. 2015.
- [10] M. Reuter, S. Biasotti, D. Giorgi, G. Patanè, and M. Spagnuolo. Discrete Laplace–Beltrami operators for shape analysis and segmentation. *Computers & Graphics*, 33(3):381–390, Jun. 2009.
- [11] Y. Lipman, R. M. Rustamov, and T. A. Funkhouser. Biharmonic distance. *ACM Transactions on Graphics (TOG)*, 29(3):27, 2010.
- [12] K. Crane, C. Weischedel, and M. Wardetzky. Geodesics in heat: A new approach to computing distance based on heat flow. *ACM Transactions on Graphics*, 32(3):10, 2013.
- [13] Y. Liu, B. Prabhakaran, and X. Guo. Point-based manifold harmonics. *IEEE Transactions on Visualization and Computer Graphics*, 18(10):1693–1703, 2012.
- [14] M. Desbrun, E. Kanso, and Y. Tong. Discrete differential forms for computational modeling. In *Discrete differential geometry*, pages 287–324. Springer, 2008.
- [15] G. Hinton and S. Roweis. Stochastic neighbor embedding. In *NIPS*, volume 15, pages 833–840, 2002.
- [16] L. van der Maaten and G. Hinton. Visualizing data using t-sne. *Journal of Machine Learning Research*, 9(Nov):2579–2605, 2008.

- [17] Y. C. Pati, R. Rezaiifar, and P. S. Krishnaprasad. Orthogonal matching pursuit: recursive function approximation with applications to wavelet decomposition. In *Proceedings of 27th Asilomar Conference on Signals, Systems and Computers*, volume 1, pages 40–44, Nov. 1993.
- [18] R. Tibshirani. Regression shrinkage and selection via the lasso. *Journal of the Royal Statistical Society. Series B (Methodological)*, pages 267–288, 1996.
- [19] M. Elad. *Sparse and Redundant Representations: From Theory to Applications in Signal and Image Processing*. Springer Publishing Company, Incorporated, 1st edition, 2010.
- [20] J. H. Friedman, J. L. Bentley, and R. A. Finkel. An algorithm for finding best matches in logarithmic expected time. *ACM Trans. Math. Softw.*, 3(3):209–226, Sep. 1977.
- [21] Jure Leskovec, Kevin J Lang, Anirban Dasgupta, and Michael W Mahoney. Community structure in large networks: Natural cluster sizes and the absence of large well-defined clusters. *Internet Mathematics*, 6(1):29–123, 2009.
- [22] J. S. Gao, A. G. Huth, M. D. Lescroart, and J. L. Gallant. Pycortex: an interactive surface visualizer for fMRI. *Frontiers in Neuroinformatics*, 9(September):1–12, 2015.
- [23] Thomas H. Cormen, Clifford Stein, Ronald L. Rivest, and Charles E. Leiserson. *Introduction to Algorithms*. McGraw-Hill Higher Education, 2nd edition, 2001.
- [24] Y. Lecun, L. Bottou, Y. Bengio, and P. Haffner. Gradient-based learning applied to document recognition. *Proceedings of the IEEE*, 86(11):2278–2324, Nov. 1998.
- [25] A. Andoni and P. Indyk. Near-optimal hashing algorithms for approximate nearest neighbor in high dimensions. *Commun. ACM*, 51(1):117–122, Jan. 2008.